JOURNAL OF SPACECRAFT AND ROCKETS
Vol. 48, No. 4, July–August 2011

# Minimum-Fuel Low-Earth-Orbit Aeroassisted Orbital Transfer of Small Spacecraft

Christopher L. Darby* and Anil V. Rao†
*University of Florida, Gainesville, Florida 32611*

DOI: 10.2514/1.A32011

**The problem of small spacecraft minimum-fuel heat-rate-constrained aeroassisted orbital transfer between two low Earth orbits with inclination change is considered. Assuming impulsive thrust, the trajectory design is described in detail and the aeroassisted orbital transfer is posed as a nonlinear optimal control problem. The optimal control problem is solved using an *hp*-adaptive pseudospectral method, and the key features of the optimal trajectories are identified. It was found that the minimum impulse solutions are obtained when the vehicle enters the atmosphere exactly twice. Furthermore, even for highly heat-rate-constrained cases, the final mass fraction of the vehicle was fairly large. Finally, the structural loads on the vehicle were quite reasonable, even in the cases where the heating rate was unconstrained.**

## Nomenclature

| | | |
|---|---|---|
| $A$ | = | vehicle reference area, $m^2$ |
| $a$ | = | semimajor axis, m |
| $C_D$ | = | coefficient of drag |
| $C_L$ | = | coefficient of drag |
| $\bar{C}_L$ | = | maximum allowable coefficient of lift |
| $D$ | = | drag specific force magnitude, $m/s^2$ |
| $e$ | = | eccentricity |
| $g_0$ | = | standard acceleration due to gravity, $m/s^2$ |
| $h$ | = | altitude over spherical Earth, m or km |
| $h_{\text{atm}}$ | = | maximum altitude of sensible atmosphere, m or km |
| $i$ | = | inclination, deg or rad |
| $K$ | = | drag polar constant |
| $L$ | = | lift specific force magnitude, $m/s^2$ |
| $\ell_{\dot{Q}}$ | = | natural logarithm of stagnation point heating rate |
| $n$ | = | number of atmospheric passes |
| $\dot{Q}$ | = | stagnation point heating rate, $W/cm^2$ |
| $\hat{\dot{Q}}$ | = | stagnation point heating-rate multiplier, $W/cm^2$ |
| $\bar{\dot{Q}}$ | = | maximum allowable stagnation point heating rate, $W/cm^2$ |
| $r$ | = | geocentric radius, m or km |
| $R_e$ | = | radius of Earth, m |
| $S$ | = | standard gravity-normalized specific force magnitude |
| $\bar{S}$ | = | maximum standard gravity-normalized specific force magnitude |
| $t$ | = | time, s or h |
| $(u_1, u_2)$ | = | alternative control parameterization |
| $v$ | = | speed, m/s or km/s |
| $v_c$ | = | Earth radius circular speed of spacecraft, m/s or km/s |
| $\alpha$ | = | angle of attack, deg or rad |
| $\bar{\alpha}$ | = | maximum allowable angle of attack, deg or rad |
| $\beta$ | = | inverse of density scale height, m/s |
| $\Delta V$ | = | instantaneous impulse, m/s or km/s |
| $\Delta V_1$ | = | instantaneous deorbit impulse, m/s or km/s |
| $\Delta V_2$ | = | instantaneous boost impulse, m/s or km/s |
| $\Delta V_3$ | = | instantaneous recircularization impulse, m/s or km/s |
| $\gamma$ | = | flight-path angle, deg or rad |
| $\theta$ | = | longitude, deg or rad |
| $\mu$ | = | gravitational parameter, $m^3/s^2$ |
| $\nu$ | = | true anomaly, deg or rad |
| $\rho$ | = | atmospheric density, $kg/m^3$ |
| $\rho_0$ | = | atmospheric density at sea level, $kg/m^3$ |
| $\sigma$ | = | bank angle, deg or rad |
| $\phi$ | = | latitude, deg or rad |
| $\psi$ | = | heading, deg or rad |
| $\Omega$ | = | longitude of ascending node, deg or rad |
| $\omega$ | = | argument of perigee, deg or rad |

Presented as Paper 2010-0102 at the 2010 AAS/AIAA Space Flight Mechanics Meeting, San Diego, CA, 15–17 February 2010; received 5 December 2010; revision received 2 February 2011; accepted for publication 22 February 2011. 

*Ph.D. Student, Department of Mechanical and Aerospace Engineering; cdarby@ufl.edu.

†Assistant Professor, Department of Mechanical and Aerospace Engineering; anilvrao@ufl.edu. Associate Fellow AIAA (Corresponding Author).

## I. Introduction

THE use of small spacecraft has been recognized in recent years as a concept that can greatly increase the operational responsiveness of space [1,2]. In particular, small spacecraft can potentially be used on short notice for rapid repositioning. To maximize operational responsiveness, it is useful for these small spacecraft to have the ability to maneuver while in the atmosphere, thus enabling these vehicles to perform an aeroassisted orbital transfer. The use of atmospheric forces can potentially enhance an onorbit maneuver (for example, inclination change) while simultaneously lowering fuel consumption, thereby reducing the overall cost of a mission as compared with using an all-propulsive orbital transfer.

Aeroassisted orbital transfer maneuvers fall into the following categories: aerobrake, aerocapture, aeroglide, aerocruise, and aerogravity assist. An aerobrake is a purely aerodynamic maneuver where the atmosphere is used to reduce the size of the orbit. An aerocapture is an atmospheric maneuver that depletes a sufficient amount of energy to change the orbit from hyperbolic to elliptic relative to the centrally attracting body. An aeroglide is a nonthrusting maneuver while the vehicle is in the atmosphere, but it is typically combined with exoatmospheric thrusting maneuvers to change the size, shape, and orientation of the orbit. An aerocruise is a maneuver that combines the use of atmospheric force with thrusting in the atmosphere. Finally, an aerogravity assist combines the atmosphere with propulsion and gravity to modify a hyperbolic orbit (i.e., an aerogravity assist is an aerodynamically assisted planet swingby).

The concept of an aeroassisted orbital transfer originates with the work of London [3]. Early work on aeroassisted orbital transfer is

summarized in the survey papers of [4,5]. Since that time, a great deal more work has been done on the problem of minimum-fuel aeroassisted orbital transfer and guidance for large spacecraft [6–17]. Hull et al. [6] considered the problem of minimum energy loss while completing an aeroassisted plane change. Seywald [7] considered the problem of optimal heating-rate-constrained solutions using an aeroassisted orbital transfer. Vinh and Shih [8] studied the problem of optimal skip trajectories using the atmosphere. Ross and Nicholson [9] considered the problem of heating-rate-constrained aerocruise maneuvers. Zimmerman and Calise [10] performed a numerical optimization study using direct collocation for the problem of low-Earth-orbit aeroassisted orbital transfer with plane change in the presence of heating rate and heat load constraints. Baumann and Oberle [11] performed a numerical optimization study of coplanar aeroassisted orbital transfer, while Baumann [12] considered the problem of aeroassisted orbital transfer with limits on thrust. Rao et al. [13] considered the problem of geostationary to low-Earth-orbit transfer using aerogliding maneuvers and multiple passes through the atmosphere in the presence of constraints on heating rate. Trask and Coverstone [14] considered coplanar and noncoplanar trajectory transfers using solar electric propulsion and aeroassisted maneuvers. Berend et al. [15] considered the problem of developing a fast method that could be used in multidisciplinary design optimization of aeroassisted orbital transfer. Gogu et al. [16] studied the sensitivity of minimum-fuel aeroassisted orbital transfer to thermal protection system mass. Finally, Berend and Bertrand [17] developed a multidisciplinary design optimization method for use in preliminary design of aeroassisted orbital transfer.

While a great deal of work has been done on aeroassisted orbital transfer for large spacecraft, the problem of aeroassisted orbital for small spacecraft has received little attention. In this research, we consider the problem of aeroassisted orbital transfer for vehicles of much smaller mass from those that have been used in previous studies (i.e., a vehicle of mass less than 1000 kg as compared with a vehicle of mass ≈5000 to 10,000 kg). Vehicles of the size considered in this research have also been considered for use in atmospheric flight trajectory design, as given in [18–20]. Using a vehicle of small mass, the objective of this research is to gain a better understanding of the performance requirements and the structure of minimum-fuel trajectories for transferring a small spacecraft between two low Earth orbits with a constraint on heating rate and a change in inclination. The optimal aeroassisted orbital transfer problem is posed as a nonlinear multiple-phase optimal control problem, and the optimal control problem is solved via direct collocation using the program General Pseudospectral Optimal Control Software (GPOPS) [21]. The overall performance of the vehicle is analyzed as a function of the number of atmospheric passes, required inclination change, and maximum allowable heating rate. Finally, the key features of the structure of the optimal trajectories are described in detail.

This paper is organized as follows. In Sec. II, we state the equations of motion and physical model for the vehicle under consideration in this study. In Sec. III, we provide a detailed description of the problem formulation. In Sec. IV, we describe the results of the numerical optimization study. In Sec. V, we provide a discussion of the results. Finally, in Sec. VI, we provide conclusions.

**Table 1 Physical and aerodynamic constants**

| Quantity | Value |
|---|---|
| $\rho_0$ | 1.225 kg/m$^3$ |
| $1/\beta$ | 7200 m |
| $A$ | 0.32 m |
| $C_{D0}$ | 0.032 |
| $K$ | 1.4 |
| $C_{L\alpha}$ | 0.5699 |
| $m_0$ | 818 kg |
| $I_{sp}$ | 310 s |
| $\hat{Q}$ | 19,987 W/cm$^2$ |
| $h_{atm}$ | 110 km |
| $R_e$ | 6,378,145 m |
| $\mu$ | $3.986 \times 10^{14}$ m$^3$/s$^2$ |
| $g_0$ | 9.80665 m/s$^2$ |

## II. Equations of Motion and Vehicle Model

The equations of motion for a vehicle in motion over a spherical nonrotating Earth are given in spherical coordinates as [13,22,23]

$$\dot{r} = v\sin\gamma, \qquad \dot{\theta} = \frac{v\cos\gamma\cos\psi}{r\cos\phi}$$
$$\dot{\phi} = \frac{v\cos\gamma\sin\psi}{r}, \qquad \dot{v} = -\frac{\rho v^2 A C_D}{2m} - \frac{\mu}{r^2}\sin\gamma$$
$$\dot{\gamma} = \frac{1}{v}\left[-\frac{\rho v^2 A}{2m}u_2 - \left(\frac{\mu}{r^2} - \frac{v^2}{r}\right)\cos\gamma\right]$$
$$\dot{\psi} = \frac{1}{v}\left[-\frac{\rho v^2 A}{2m\cos\gamma}u_1 - \frac{v^2}{r}\cos\gamma\cos\psi\tan\phi\right] \tag{1}$$

The atmospheric density and aerodynamic coefficients are modeled, respectively, as [22]

$$\rho = \rho_0\exp(-\beta h), \qquad C_L = C_{L\alpha}\alpha, \qquad C_D = C_{D0} + KC_L^2 \tag{2}$$

where $h = r - R_e$. In this study, we choose a high lift-to-drag vehicle of small mass similar to that studied in [24]. The aerodynamic data for this vehicle, along with the physical constants, are shown in Table 1. It is noted that $u_1$ and $u_2$ correspond to the quantities

$$u_1 = -C_L\sin\sigma, \qquad u_2 = -C_L\cos\sigma \tag{3}$$

where $\sigma = \tan^{-1}(u_2, u_1)$, and $\tan^{-1}$ is the four-quadrant inverse tangent function. It is noted that $C_L$ and $C_D$ are omitted from Eq. (1) during exoatmospheric flight. Furthermore, we note that no constraints are placed on the relative position between the spacecraft and a particular point on the Earth, and the trajectory transfer time is small. Thus, for the purposes of this study, a nonrotating Earth model is sufficient. Finally, it is noted that, qualitatively, results obtained in this research will not change using a higher-fidelity gravity model; thus, a spherical gravity model is used.

## III. Problem Formulation

In this section, we formulate the problem of transferring a small spacecraft, for which the model is given in Sec. II, between two low Earth orbits with an inclination change and a constraint on the heating rate while minimizing the fuel consumption. The components required for this orbital transfer are developed as follows. In Sec. III.A, we formulate the trajectory event sequence. In Sec. III.B, we provide the initial and terminal conditions. In Sec. III.C, we develop the interior point constraints. In Sec. III.D, we formulate the path constraints during flight. In Sec. III.E, we develop the objective functional that is to be minimized.

### A. Trajectory Event Sequence

Let $n$ be the number of atmospheric passes during the orbital transfer. The trajectory event sequence for an $n$-pass transfer is as follows. First, the following phases and events initiate the transfer (see Fig. 1a):

1) An event occurs where a deorbit impulse is applied from the initial orbit defined by Eq. (4).

2) A phase occurs where an exoatmospheric flight segment terminates at the edge of the sensible atmosphere $h_{atm}$.

3) A phase occurs where an atmospheric flight segment terminates at the edge of the sensible atmosphere $h_{atm}$.

The following two phases are then repeated for the remaining $n-1$ atmospheric passes (see Fig. 1b):

4) A phase occurs where an exoatmospheric flight segment terminates at the edge of the sensible atmosphere $h_{atm}$.

5) A phase occurs where an atmospheric flight segment terminates at the edge of the sensible atmosphere $h_{atm}$.

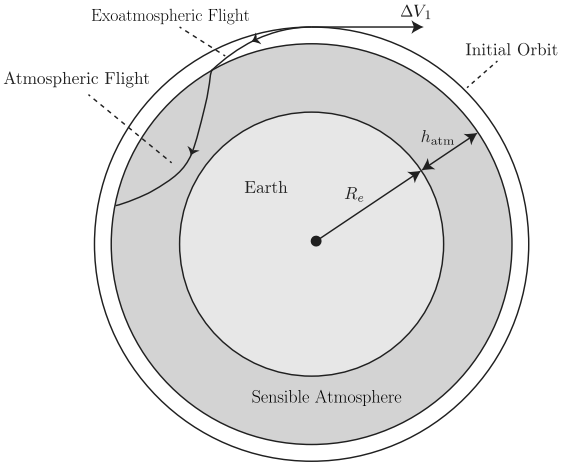


**a) Initial phases of trajectory design**

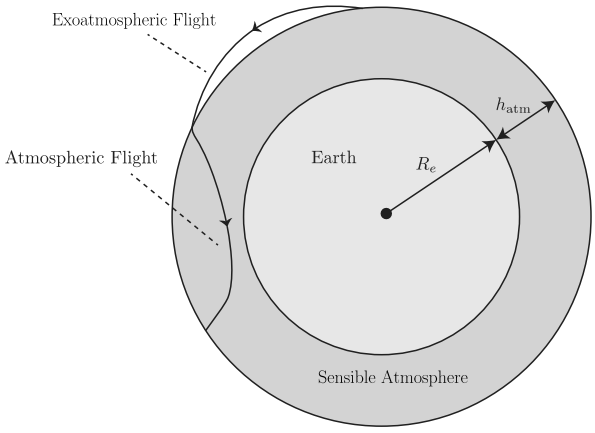


**b) Intermediate phases of trajectory design**

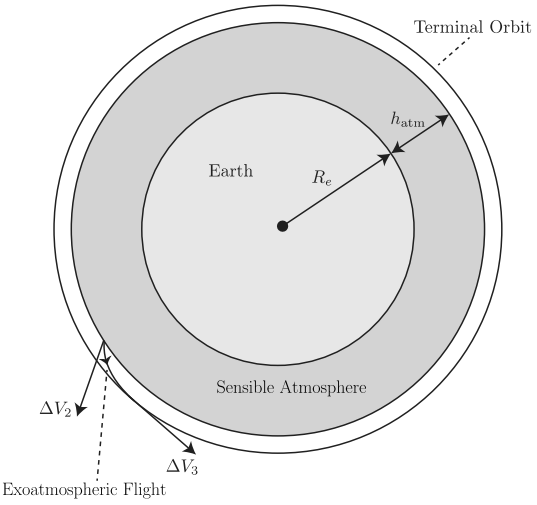


**c) Final phase of trajectory design**

**Fig. 1 Schematic of trajectory design for aeroassisted orbital transfer problem.**

Finally, the trajectory terminates with the following three phases and events (see Fig. 1c):

6) An event occurs where an impulse is applied at the maximum altitude of the sensible atmosphere.

7) A phase occurs where an exoatmospheric flight segment terminates at the final orbital altitude.

8) An event occurs where an impulse is applied at the final orbital altitude to recircularize the orbit.

### B. Initial and Terminal Conditions

The initial conditions correspond to those of an equatorial circular orbit of altitude $h_0$. This initial orbit is given in terms of orbital elements as

$$\begin{aligned} &a(t_0) = R_e + h_0, \qquad e(t_0) = 0 \qquad i(t_0) = 0, \qquad \Omega(t_0) = 0 \\ &\omega(t_0) = 0, \qquad \nu(t_0) = 0 \end{aligned} \tag{4}$$

where the values for $\Omega(t_0)$, $\omega(t_0)$, and $\nu(t_0)$ are arbitrarily set to zero. The terminal conditions correspond to a circular orbit of altitude $h_f$ and are given as

$$a(t_f) = R_e + h_f, \qquad e(t_f) = 0, \qquad i(t_f) = i_f \tag{5}$$

where $i_f$ is the prescribed inclination of the terminal orbit. Because the terminal orbit is circular and no constraints are placed on the location of the spacecraft in the terminal orbit, the values $\Omega(t_f)$ and $\omega(t_f)$ are undefined while the value $\nu(t_f)$ is free.

### C. Interior Point Constraints

The following interior point constraints are imposed at each entry and exit to the atmosphere. First, in order to ensure that the vehicle is descending upon atmospheric entry, the following constraints are imposed at each atmospheric entry:

$$r(t_0^{\text{atm}}) = h_{\text{atm}} + R_e, \qquad \gamma(t_0^{\text{atm}}) \leq 0 \tag{6}$$

where $t_0^{\text{atm}}$ is the time at the start of any atmospheric flight segment. Next, in order to ensure that the vehicle is ascending upon atmospheric exit, the following constraint is imposed at each atmospheric exit:

$$r(t_f^{\text{atm}}) = h_{\text{atm}} + R_e, \qquad \gamma(t_f^{\text{atm}}) \geq 0 \tag{7}$$

where $t_f^{(\text{atm})}$ is the time at the terminus of any atmospheric flight segment.

### D. Vehicle Path Constraints

The following three inequality path constraints are enforced on the vehicle during atmospheric flight. First, the angle of attack is constrained as

$$0 \leq \alpha \leq \bar{\alpha} \tag{8}$$

We note, however, because the coefficient of lift is linear in $\alpha$, it is more convenient to constrain $C_L$ as

$$0 \le C_L \le \bar{C}_L \tag{9}$$

Consequently, the controls $u_1$ and $u_2$ given in Eq. (3) must satisfy the inequality constraints

$$-\bar{C}_L \le u_i \le \bar{C}_L, \qquad (i = 1, 2) \tag{10}$$

In addition, using the fact that $u_1^2 + u_2^2 = C_L^2$ together with Eq. (9), we have

$$0 \le u_1^2 + u_2^2 \le \bar{C}_L^2 \tag{11}$$

In this research, the maximum coefficient of lift is $\bar{C}_L = 0.4$, which corresponds to a maximum angle of attack $\bar{\alpha} \approx 40$ deg.

Next, a constraint is placed on the stagnation point heating rate. Using the Chapman equation [25], the stagnation point heating rate, denoted as $\dot{Q}$, is computed as

$$\dot{Q} = \hat{\dot{Q}}(\rho/\rho_0)^{0.5}(v/v_c)^{3.15} \tag{12}$$

where $v_c = \sqrt{\mu/R_e}$. Because $\dot{Q}$ is always positive during atmospheric flight, it can be transformed monotonically via the natural logarithm as

$$\ell_{\dot{Q}} = \log \dot{Q} = \log \hat{\dot{Q}} - \beta h/2 + 3.15 \log(v/v_c) \tag{13}$$

where we have used Eq. (2) to obtain the result of Eq. (13). Computationally, Eq. (13) is better behaved in the optimization than the original constraint of Eq. (12). Finally, we constrain the altitude during atmospheric entry to be $0 \le h \le h_{\text{atm}}$, which implies that $R_e \le r \le h_{\text{atm}} + R_e$. Thus, the following five inequality path constraints are imposed during atmospheric flight:

$$\begin{gathered} -\bar{C}_L \le u_1 \le \bar{C}_L, \quad -\bar{C}_L \le u_2 \le \bar{C}_L, \quad -\infty \le \ell_{\dot{Q}} \le \log \bar{\dot{Q}} \\ 0 \le u_1^2 + u_2^2 \le \bar{C}_L^2, \quad R_e \le r \le h_{\text{atm}} + R_e \end{gathered} \tag{14}$$

where $\bar{\dot{Q}}$ is the maximum allowable value of the stagnation point heating rate.

### E. Performance Index

The objective of the aerogliding maneuver is to minimize the fuel consumed during the transfer. Assuming impulsive thrust maneuvers, the instantaneous impulse $\Delta V$ is a direct measure of the fuel consumed during a thrusting maneuver. The objective is then to minimize the sum of the magnitudes of the impulses during the transfer: that is, to minimize the cost functional

$$J = \sum_{i=1}^{3} \Delta V_i \tag{15}$$

where we recall that $\Delta V_1$, $\Delta V_2$, and $\Delta V_3$ are the deorbit, boost, and recircularization impulses, respectively, as shown in Figs. 1a–1c. The mass lost due to the application of an instantaneous impulse can then be computed from the Goddard rocket equation as

$$\Delta V = g_0 I_{\text{sp}} \ell_n(m^+/m^-) \tag{16}$$

where $m^+$ and $m^-$ are the values of the mass immediately before and after application of the impulse. An equivalent cost can be formulated to maximize the final mass of the vehicle; that is, minimize

$$J = -m(t_f) \tag{17}$$

While either Eq. (15) or Eq. (17) can be used, in this research, we use Eq. (17) for the objective functional.

### F. Optimal Control Problem

The optimal control problem that corresponds to the trajectory design given in Sec. III.A is now stated as follows. Determine the trajectory $[r(t), \theta(t), \phi(t), v(t), \gamma(t), \psi(t)]$, the controls $[u_1(t), u_2(t)]$,

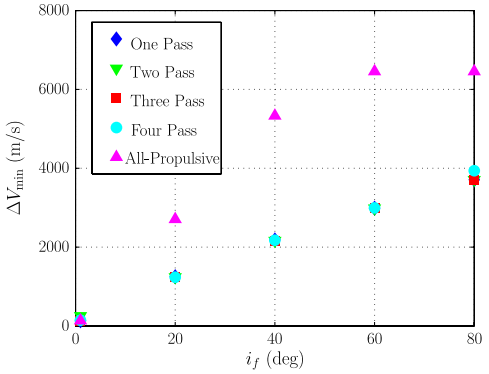


**a) $\Delta V_{\min}$ vs $i_f$**

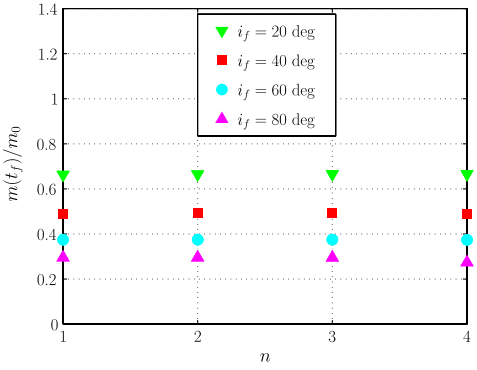


**b) $m(t_f)/m_0$ vs $n$**

**Fig. 2 Minimum impulse $\Delta V_{\min}$ vs final inclination $i_f$, and final mass fraction $m(t_f)/m_0$ vs number of atmospheric passes $n$ for heating-rate-unconstrained aeroassisted orbital transfer.**

and the impulses $(\Delta V_1, \Delta V_2, \Delta V_3)$ that minimize the cost functional of Eq. (17) subject to the dynamic constraints of Eqs. (1), the initial and terminal constraints given in Eqs. (4) and (5), the interior point constraints of Eqs. (6) and (7), and the path constraints of Eq. (14). The optimal control problem was solved in canonical units, where length is measured in Earth radii, time is measured in units of $\sqrt{R_e^3/\mu}$, speed is measured in units of $\sqrt{\mu/R_e}$, and mass is measured in units of the initial mass of the vehicle $m_0$. The optimal control problem is solved using the $hp$-adaptive version of the open-source pseudospectral optimal control software GPOPS [21,26,27] with the MATLAB version of the nonlinear programming problem (NLP) solver SNOPT [28,29] using default feasibility and optimality tolerances. Moreover, all NLP derivatives were computed using the MATLAB automatic differentiator INTLAB (interval laboratory) [30]. The $hp$-adaptive version of GPOPS implements the Radau pseudospectral method, as described extensively in [31,32], together with the $hp$-adaptive mesh algorithm, detailed in [26]. The mesh refinement algorithm determines iteratively the number of mesh intervals and the number of collocation points. On each mesh, the errors in the solution are assessed by determining how accurately the differential equation and path constraints are satisfied between the collocation points. The mesh refinement terminates when a grid is obtained that satisfies the accuracy tolerances. In this research, the $hp$-adaptive accuracy tolerances were three orders of magnitude less than the SNOPT feasibility tolerance.

**Table 2 Aeroassisted $\Delta V_{\min}$ for small inclination changes with $n = 1$ and no constraint on heating rate alongside all-propulsive $\Delta V_{\min}$**

| $i_f$, deg | Aeroassisted $\Delta V_{\min}$, m/s | All-propulsive $\Delta V_{\min}$, m/s |
|---|---|---|
| 1 | 131.7 | 136.0 |
| 2 | 281.7 | 272.0 |
| 3 | 354.0 | 408.0 |
| 4 | 411.1 | 543.9 |
| 5 | 467.7 | 680.0 |

## IV. Results

The aeroassisted orbital transfer problem described in Sec. IV was solved using GPOPS [26,21,27] for $n = (1, 2, 3, 4)$, $\dot{\bar{Q}} = (400, 800, 1200, \infty)$ W/cm$^2$, $i_f = (1, 20, 40, 60, 80)$ deg, and $h_0 = h_f = 185.2$ km (100 n mile). For completeness, we compare the results obtained using the aeroassisted orbital transfer against the following typical all-propulsive maneuvers: 1) a direct change in inclination via rotation of the initial velocity and 2) a biparabolic transfer. It is noted that the biparabolic transfer is an idealization of a bielliptic transfer where the apogee of the elliptic transfer orbit is $\infty$. For initial and terminal circular orbits of the same size, but with different inclinations, the direct and biparabolic impulses required to change inclination by an amount $\Delta i$ are given, respectively, as [33]

$$\Delta V = 2v_0 \sin \Delta i/2, \qquad \Delta V = 2(\sqrt{2} - 1)v_0 \tag{18}$$

where $v_0$ is the initial orbital speed. It is known that the biparabolic transfer is more efficient for $\Delta i > 49$ deg. Therefore, in our analysis, we will compare the aeroassisted orbital transfer fuel consumption against the single impulse maneuver when $\Delta i \leq 49$ deg and against the biparabolic transfer when $\Delta i > 49$ deg.

### A. Overall Performance

#### 1. *Heating-Rate-Unconstrained Solutions*

Figure 2a shows the minimum total impulse $\Delta V_{\min}$ for the heating-rate-unconstrained aeroassisted maneuvers alongside the all-propulsive maneuvers as a function of $i_f$. First, examining Fig. 2a, it is seen that aeroassisted minimum impulse is highly insensitive to the number of atmospheric passes $n$ for any given value of $i_f$. Next, it is apparent from Fig. 2a that the aeroassisted minimum impulse is much more fuel efficient than the all-propulsive minimum impulse for larger values of $i_f$. Next, Table 2 shows the trends in $\Delta V_{\min}$ for small values of $i_f$ in the case where $n = 1$. It is seen from Table 2 that the minimum impulse for the aeroassisted and all-propulsive maneuvers are essentially the same until $i_f$ is between 2 and 3 deg. For $i_f > 3$ deg, it is seen that the aeroassisted and all-propulsive $\Delta V_{\min}$ diverge. Finally, Fig. 2b shows the final mass fraction, $m(t_f)/m_0$, for $i_f = (20, 40, 60, 80)$ deg, where it is seen that an inclination change of 80 deg can be accomplished while retaining slightly less than 30% of the initial mass in the case that the vehicle that can withstand any heating rate during atmospheric entry.

In addition to the total $\Delta V_{\min}$, it is interesting to see how the minimum impulse is divided between deorbit $\Delta V_1$, boost $\Delta V_2$, and recircularization $\Delta V_3$. Specifically, Figs. 3a–3c show that the deorbit and recircularization impulses are significantly smaller than the boost impulse. Next, Fig. 3d shows the impulse lost to drag $\Delta V_D$ in the atmosphere as a function of $n$ and $i_f$. As might be expected, the boost impulse $\Delta V_2$ essentially compensates for the velocity loss during the atmospheric maneuver. Thus, for a given inclination change, the increase in $\Delta V_{\min}$ for any number of passes is dominated by the need to apply more impulse to overcome velocity loss due to atmospheric drag. Next, Fig. 4a shows the total inclination change accomplished by aerodynamic forces $\Delta i_{\text{aero}}$ as a function of the number of atmospheric passes. It is seen that the amount of inclination change performed by the atmosphere is essentially constant as the function of the number of atmospheric passes. This last result implies that entering the atmosphere multiple times does not improve the amount of inclination change that is possible over a single atmospheric pass when the heating rate is unconstrained. Furthermore, because $\Delta V_1$ and $\Delta V_3$ are each two orders of magnitude smaller than $\Delta V_2$, the exoatmospheric portion of the inclination change is performed almost exclusively with $\Delta V_2$. Finally, Fig. 4b shows the total trajectory time as a function of the number of atmospheric passes. As may be expected, the transfer time increases as a function of $n$.

#### 2. *Heating-Rate-Constrained Solutions*

Figures 5a–5d show the total minimum impulse $\Delta V_{\min}$ as a function of the number of atmospheric passes $n$, $\dot{\bar{Q}}$, and $i_f$, while Figs. 6a–6d show the corresponding results for the final mass fraction, $m(t_f)/m_0$. Similar to the heating-rate-unconstrained

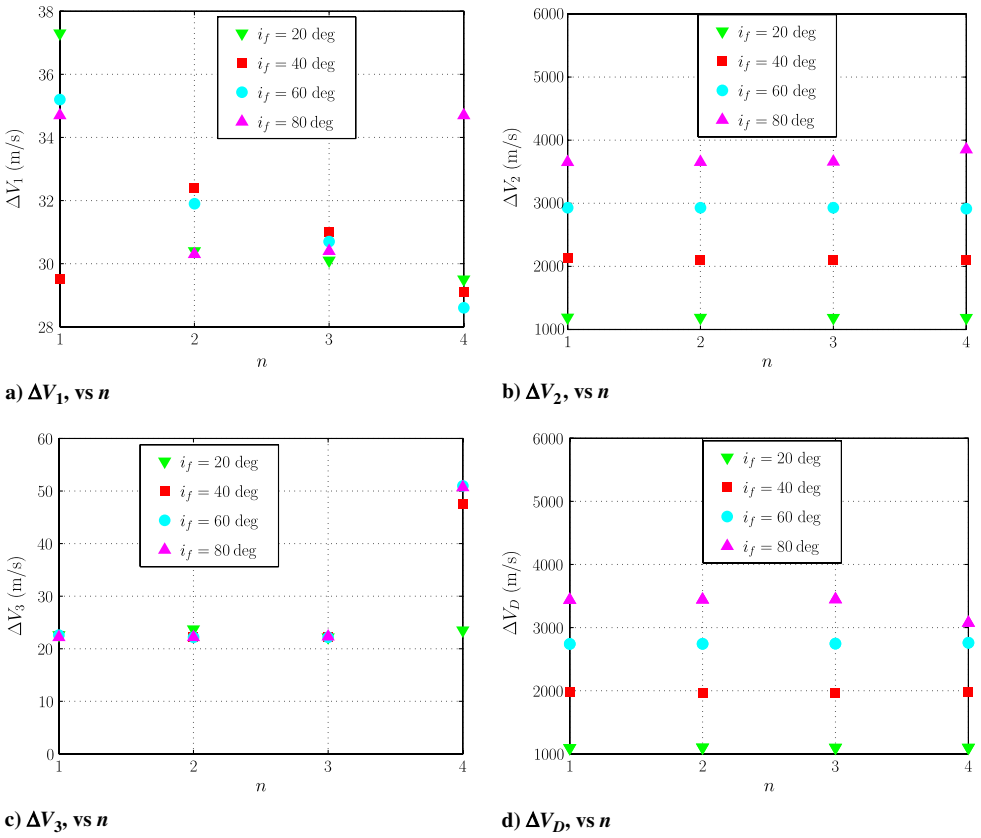


**a) $\Delta V_1$, vs $n$** **b) $\Delta V_2$, vs $n$**

**c) $\Delta V_3$, vs $n$** **d) $\Delta V_D$, vs $n$**

**Fig. 3 Deorbit $\Delta V_1$, boost $\Delta V_2$, recircularization $\Delta V_3$, and drag $\Delta V_D$ impulses as functions of number of atmospheric passes $n$ for heating-rate-unconstrained aeroassisted orbital transfer.**

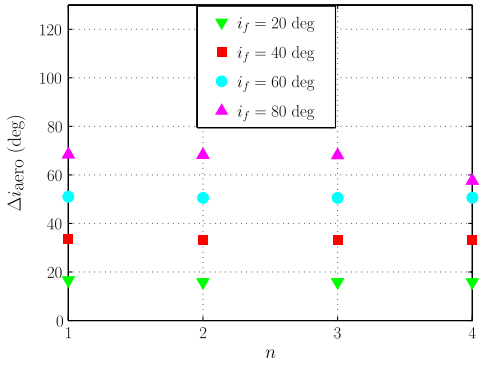


**a) $\Delta i_{\text{aero}}$ vs $n$**

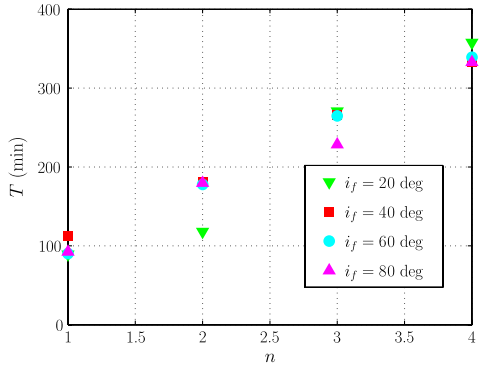


**b) $T$ vs $n$**

**Fig. 4 Inclination change performed by atmosphere $\Delta i_{\text{aero}}$ and trajectory transfer time $T$ vs number of atmospheric passes $n$ for heating-rate-unconstrained aeroassisted orbital transfer.**

solutions, it is seen that $\Delta V_{\text{min}}$ is insensitive to the number of atmospheric passes, but it increases noticeably as $\bar{\dot{Q}}$ decreases. In addition, Figs. 5a–5d shows that the difference in $\Delta V_{\text{min}}$ between the aeroassisted and all-propulsive maneuvers decreases with decreasing maximum allowable heating rate $\bar{\dot{Q}}$. Finally, it is seen for the case where $\bar{\dot{Q}} = 400$ W/cm$^2$ and $i_f = 60$ deg that the final mass fraction is $\approx$0.17, which is still 7% higher than the all-propulsive maneuver, while for the case $\bar{\dot{Q}} = 400$ W/cm$^2$ and $i_f = 80$ deg, the final mass fraction is $\approx$0.08, which is 2% lower than that of the all-propulsive maneuver. Thus, the all-propulsive maneuver is slightly more fuel efficient than the aeroassisted maneuver when the heating rate is highly constrained and the desired inclination change is very large.

Next, let $S$ be the sea level gravity-normalized specific force, defined as

$$S = \frac{\rho v^2 A}{2mg_0}\sqrt{C_D^2 + C_L^2} \tag{19}$$

Figures 7a–7d show the maximum value of $S$, denoted as $\bar{S}$, as a function of the number of atmospheric passes $\bar{\dot{Q}}$, and $i_f$. It is seen that, when the heating rate is unconstrained, $S$ varies between $\approx$4 for $i_f = 20$ deg and $\approx$17 g for $i_f = 60$ deg. On the other hand, when the heating rate is highly constrained, $S < 1$, which implies that the maximum specific force $g_0 S$ is less than the standard acceleration due to gravity. The results of Figs. 6a–6d and 7a–7c show that a fully loaded vehicle of mass $m_0 = 818$ kg (used in this study) would be able to complete a 60 deg highly heating-rate-constrained maneuver and still be left with a dry mass as large as $\approx$140 kg.

### B. Structure of Optimal Trajectories

The key features of the trajectories are seen by examining the solutions obtained for one atmospheric pass, $n = 1$, and a 40 deg inclination change, $i_f = 40$ deg, for different values of $\bar{\dot{Q}}$ and comparing these solutions with the solutions obtained for $n > 1$. First, Figs. 8a and 8b show $h$ vs $v$ and $\dot{Q}$ vs $t$, respectively, for

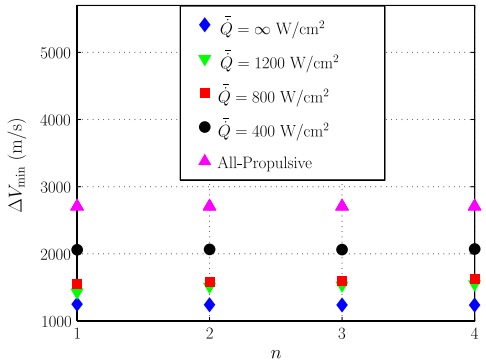


**a) $\Delta V_{\text{min}}$ vs $n$ for $i_f$ = 20 deg**

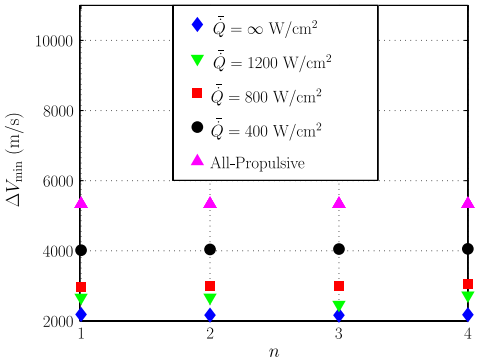


**b) $\Delta V_{\text{min}}$ vs $n$ for $i_f$ = 40 deg**

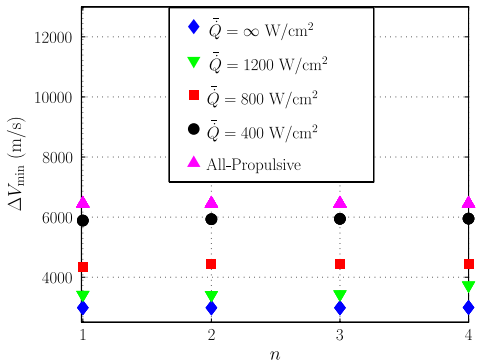


**c) $\Delta V_{\text{min}}$ vs $n$ for $i_f$ = 60 deg**

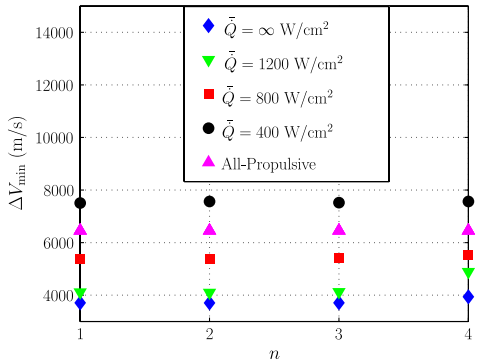


**d) $\Delta V_{\text{min}}$ vs $n$ for $i_f$ = 80 deg**

**Fig. 5 Minimum impulse $\Delta V_{\text{min}}$ vs number of atmospheric passes $n$ for different maximum allowable heating rates and final inclinations.**

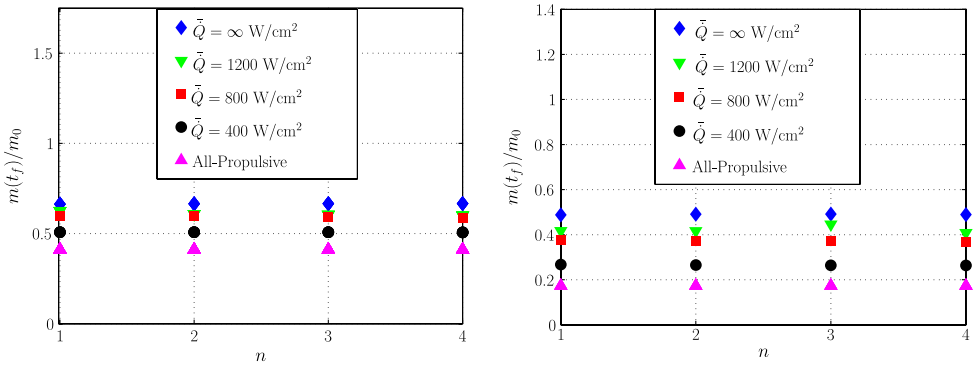


a) $m(t_f)/m_0$ vs $n$ for $i_f = 20$ deg

b) $m(t_f)/m_0$ vs $n$ for $i_f = 40$ deg

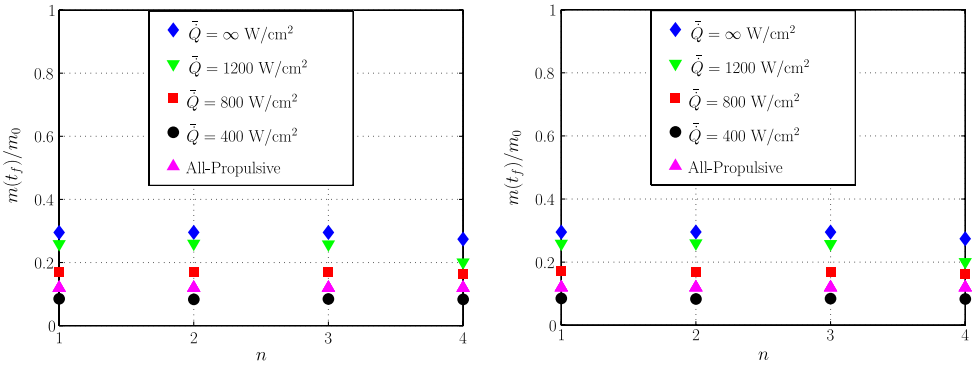


c) $m(t_f)/m_0$ vs $n$ for $i_f = 60$ deg

d) $m(t_f)/m_0$ vs $n$ for $i_f = 80$ deg

**Fig. 6 Final mass fraction $m(t_f)/m_0$ vs number of atmospheric passes, maximum allowable heating rate $\bar{\dot{Q}}$, and final inclination $i_f$.**

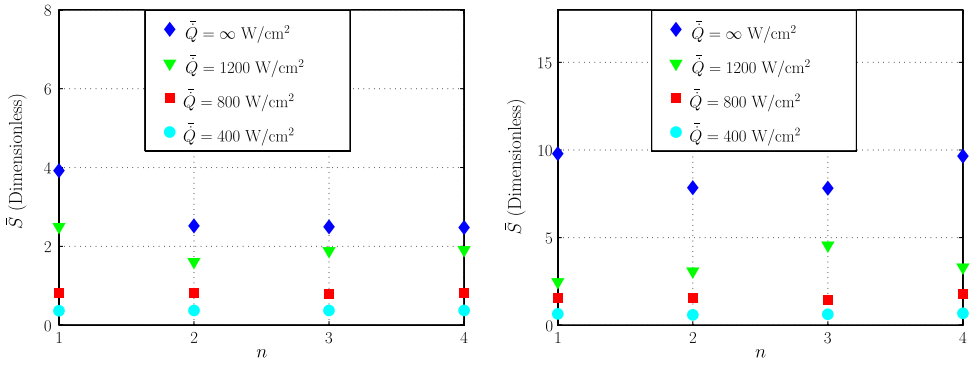


a) $\bar{S}$ vs $n$ for $i_f = 20$ deg

b) $\bar{S}$ vs $n$ for $i_f = 40$ deg

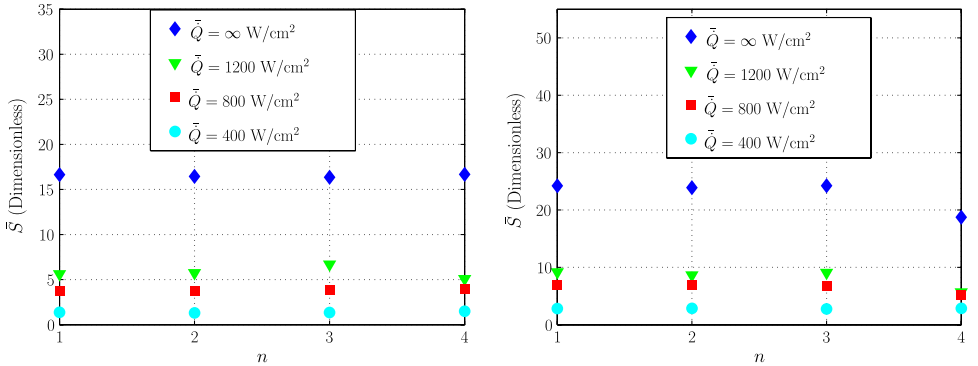


c) $\bar{S}$ vs $n$ for $i_f = 60$ deg

d) $\bar{S}$ vs $n$ for $i_f = 80$ deg

**Fig. 7 Maximum standard gravity-normalized specific force $\bar{S}/g_0$ vs number of atmospheric passes $n$, maximum allowable heating rate $\bar{\dot{Q}}$, and final inclination $i_f$.**

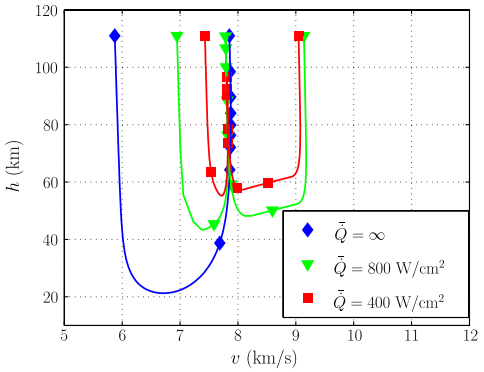


a) $h$, vs $v$ for $i_f = 40$ deg

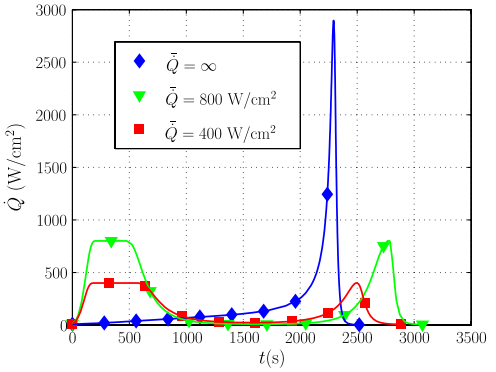


b) $\dot{Q}$, vs $t$ for $i_f = 40$ deg

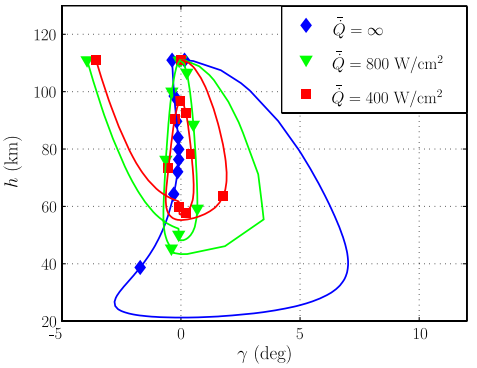


c) $h$ vs $\gamma$ for $i_f = 40$ deg

**Fig. 8 Altitude $h$ vs speed $v$, and heating rate $\dot{Q}$ vs time $t$ for $i_f = 40$ deg.**

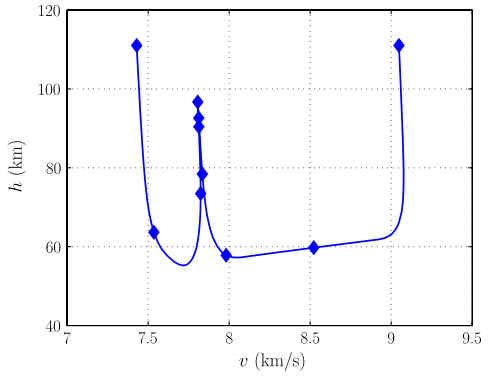


a) $h$ vs $v$ for $n = 1$ and $i_f = 40$ deg

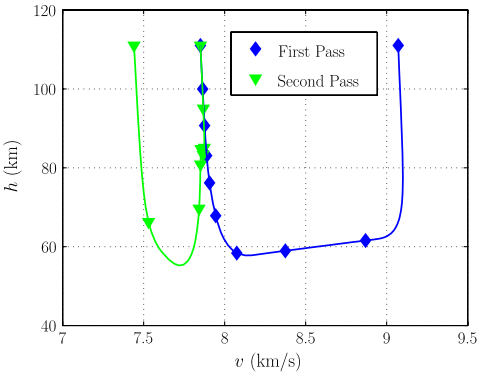


b) $h$ vs $v$ for $n = 2$ and $i_f = 40$ deg

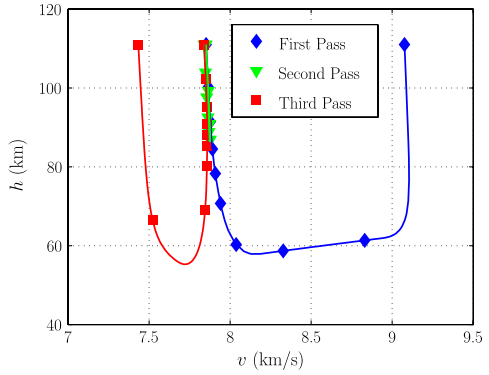


c) $h$ vs $v$ for $n = 3$ and $i_f = 40$ deg

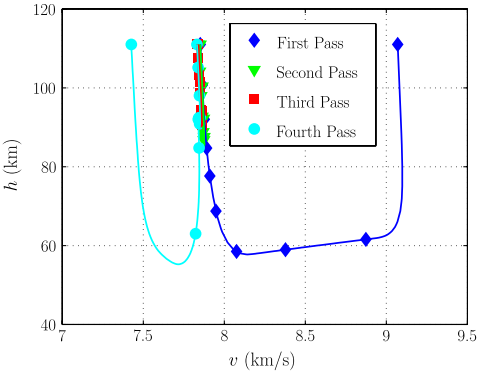


d) $h$ vs $v$ for $n = 4$ and $i_f = 40$ deg

**Fig. 9 Altitude $h$ vs speed $v$ for $n = (1, 2, 3, 4)$, $i_f = 40$ deg, and $\bar{\dot{Q}} = 400$ W/cm$^2$.**

$\bar{\dot{Q}} = (\infty, 400, 800)$ W/cm$^2$. It is interesting to observe the difference between the behavior of the optimal solution for the unconstrained and constrained heating-rate cases. In the case where the heating rate is unconstrained, the vehicle enters the atmosphere once, whereas in the case where the heating rate is constrained, the natural solution is for the vehicle to enter the atmosphere twice. The fact that the optimal solution uses two atmospheric passes is seen in Fig. 8a, where although we have set $n = 1$, the vehicle descends into the atmosphere twice while reascending to near the edge of the sensible atmosphere, $h = h_{\text{atm}}$, between the two descents. Although one might expect that the vehicle would only descend into the atmosphere once for $n = 1$, when we solved the problem by forcing a single descent into the atmosphere, we obtained a higher cost. Next, Fig. 8c shows $h$ vs $\gamma$. In this case, it is seen for the case where $\dot{Q}$ is unconstrained that the atmospheric flight contains an equilibrium glide segment where the altitude changes at a nearly constant flight-path angle. In the case where the heating rate is constrained, however, an equilibrium glide segment does not exist.

The observation that the optimal heating-rate-constrained solution for $n = 1$ is actually to use the atmosphere twice suggests that the structure of the optimal heating-rate-constrained solutions for $n > 2$ may simply reduce to the optimal solution for $n = 2$. To test this hypothesis, the structure of the optimal solutions for more than two atmospheric passes was examined in more detail. Figures 9a–9d show $h$ vs $v$ for $n = (1, 2, 3, 4)$, $i_f = 40$ deg, and $\bar{\dot{Q}} = 400$ W/cm$^2$. First, it is seen that the solution for $n = 2$ is identical to that for $n = 1$, demonstrating that adding a second atmospheric pass is the same as allowing for a single atmospheric pass, because the vehicle performs the same maneuver in either case. Next, the solutions for $n = (3, 4)$ are again essentially the same as those obtained for either $n = 1$ or $n = 2$, because the altitude during an intermediate pass through the atmosphere is never low enough to effect an inclination change. The negligible effect of using more than two atmospheric passes is further validated by examining the heating rate during atmospheric entry. Specifically, Figs. 10a–10d show that the structure of $\dot{Q}$ for $n = 1$ is essentially identical to the structure of $\dot{Q}$ for $n = (2, 3, 4)$. In particular, Figs. 10b and 10c show that the maximum value of $\dot{Q}$ during the intermediate atmospheric passes (i.e., the second atmospheric pass for $n = 3$ and the second and third atmospheric passes for $n = 4$) are extremely small, rendering these atmospheric passes insignificant. It is interesting to observe that the structure of the optimal trajectory for $n = 1$ is the same as that for $n = (2, 3, 4)$: the only difference being the total trajectory transfer time due to the fact that we are requiring more atmospheric entries when $n = (3, 4)$ as compared with when $n = 2$ (which, we reemphasize, is equivalent to $n = 1$ for the case where the heating rate is constrained). Finally, it is seen from Figs. 11a–11d that the location of the maximum specific force exerted on the vehicle is coincident with the location of the maximum heating rate.

Next, we examine the structure of the controls $\alpha$ and $\sigma$. Figures 12a and 12b show $\alpha$ and $\sigma$, respectively, vs $t$ for $n = 1$, $i_f = 40$, and various values of $\bar{\dot{Q}}$. As may be expected, $\alpha$ attains its maximum value of 40 deg near the regions of atmospheric flight where the heating rate is large. Furthermore, it is seen that the vehicle enters the atmosphere with $\sigma \approx 100$ deg and leaves the atmosphere with $\sigma \approx -100$ deg. This behavior in the bank angle is consistent with the need to increase inclination upon atmospheric entry (thereby requiring that the bank angle be $\approx 90$ deg at atmospheric entry) and align the velocity with the plane of the terminal orbit upon atmospheric exist (thereby requiring that the bank angle be $\approx -90$ deg at atmospheric exit).

## V. Discussion

The results of this study highlight several interesting aspects of using aerogliding maneuvers to change the inclination of a vehicle in low Earth orbit. First, it is seen that a relatively small upper limit (approximately 400 W/cm$^2$) can be placed on the heating rate during atmospheric entry while still providing a final mass fraction $m(t_f)/m_0 \approx 0.17$. Second, it is seen that the natural minimum-

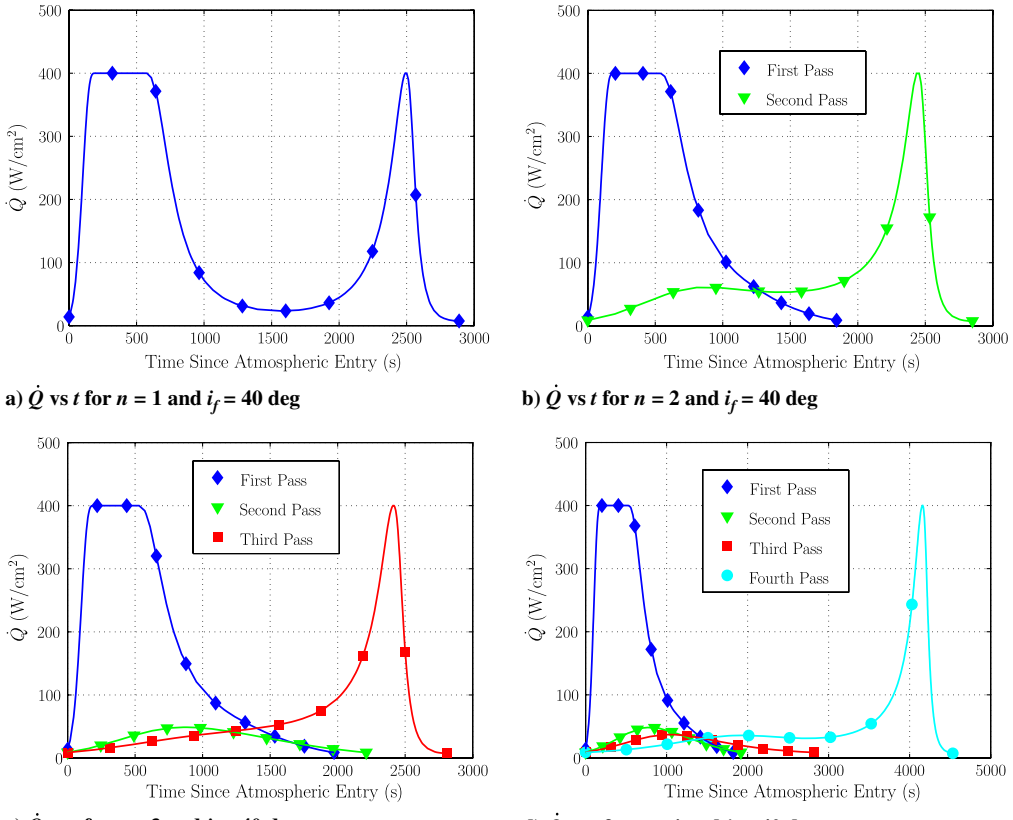


**a) $\dot{Q}$ vs $t$ for $n = 1$ and $i_f = 40$ deg**

**b) $\dot{Q}$ vs $t$ for $n = 2$ and $i_f = 40$ deg**

**c) $\dot{Q}$ vs $t$ for $n = 3$ and $i_f = 40$ deg**

**d) $\dot{Q}$ vs $t$ for $n = 4$ and $i_f = 40$ deg**

**Fig. 10 Heating rate $\dot{Q}$ vs time $t$ for $n = (1, 2, 3, 4)$, $i_f = 40$ deg, and $\bar{\dot{Q}} = 400$ W/cm$^2$.**

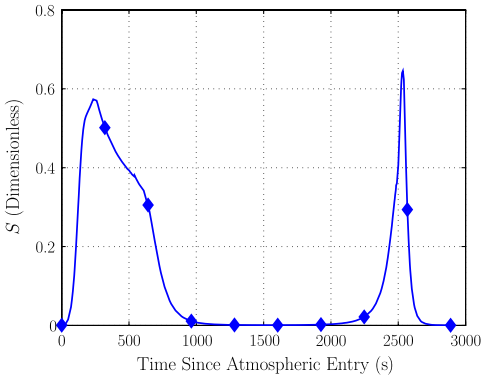


a) $S$ vs $t$ for $n = 1$ and $i_f = 40$ deg

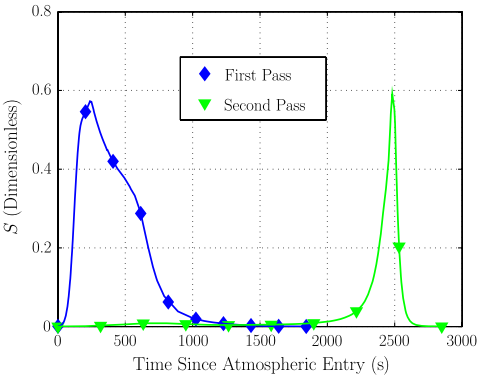


b) $S$ vs $t$ for $n = 2$ and $i_f = 40$ deg

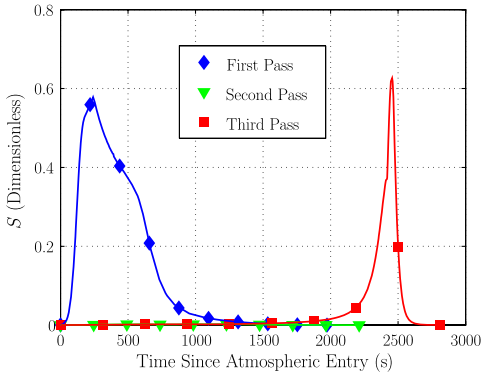


c) $S$ vs $t$ for $n = 3$ and $i_f = 40$ deg

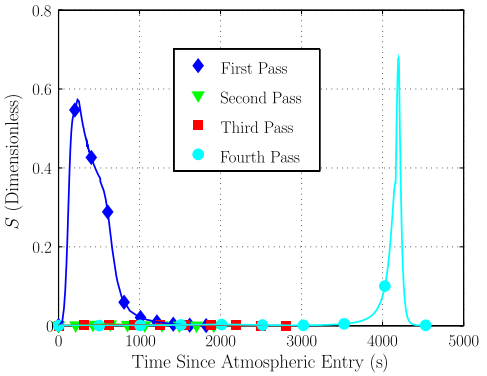


d) $S$ vs $t$ for $n = 2$ and $i_f = 40$ deg

**Fig. 11 Standard gravity-normalized specific force $S$ vs time $t$ for $n = (1, 2, 3, 4)$, $i_f = 40$ deg, and $\bar{\dot{Q}} = 400$ W/cm$^2$.**

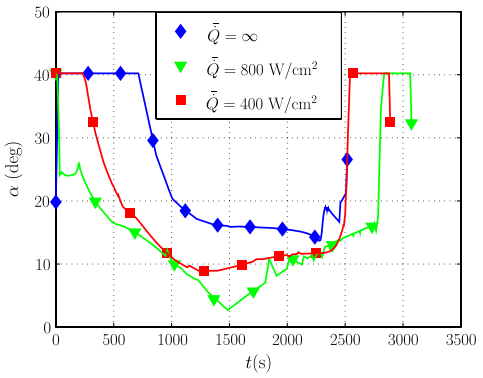


a) $\alpha$ vs $t$ for $n = 1$ and $i_f = 40$ deg

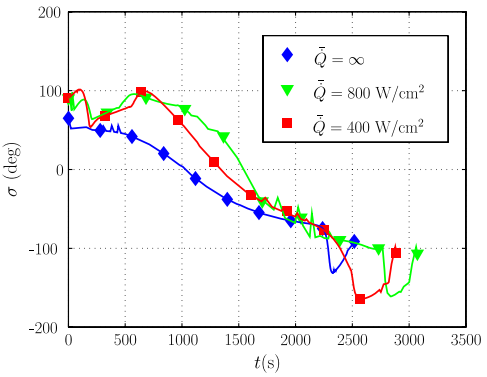


b) $\sigma$ vs $t$ for $n = 1$ and $i_f = 40$ deg

**Fig. 12 Angle of attack $\alpha$ and bank angle $\sigma$ vs time for $n = 1$ and $i_f = 40$ deg.**

impulse solution in the presence of a heating-rate constraint is to use two passes through the atmosphere. The first atmospheric pass contains a segment that lies on the heating-rate constraint, while the second pass only touches the heating rate for an instant of time. Moreover, the structure of the heating-rate-constrained solutions is the same for two or more atmospheric passes. Finally, it is seen that the minimum impulse obtained using the aerogliding maneuver is significantly less than either a direct or biparabolic all-propulsive maneuver.

It is also interesting to contrast the results obtained in this study as compared with those obtained in [13]. In particular, [13] studies the problem of minimum-fuel aerogliding maneuvers from geostationary orbit to low Earth orbit for a much more massive vehicle from the one considered in this study. For the vehicle used in this study, the results of Sec. IV show that the minimum impulse is obtained using exactly two atmospheric entries. In the work of [13], however, the minimum $\Delta V$ decreases as the number of entries into the atmosphere increases. Thus, when a more massive vehicle is used to make a large change to the size and inclination of the orbit, it is advantageous to use a large number of atmospheric passes over using a single atmospheric pass. Finally, it is noted that [13] considers a trajectory design that includes exoatmospheric impulses between atmospheric flight segments. It was found in [13], however, that the intermediate exoatmospheric impulses were negligible. As a result, when conceiving the trajectory design for this research, intermediate impulses were not included in the trajectory design.

## VI. Conclusions

The problem of transferring a small high lift-to-drag ratio vehicle between two low Earth orbits using aeroassisted maneuvers has been considered. A trajectory has been designed that includes deorbit, boost, and recircularization impulses together with atmospheric flight segments. The trajectory design was optimized by numerically solving a nonlinear optimal control using an $hp$-adaptive pseudospectral method. It was found that the natural optimal solution

to the problem was to perform two adjacent passes through the atmosphere, where the first pass was at the heating-rate limit for a nonzero duration, while the second pass only touched the heating-rate constraint for an instant. When more than two atmospheric passes were used and the heating rate was constrained, all solutions reduced to the two-pass solution. It was also found that the final mass fraction was still fairly large, even in the case where the heating rate was highly constrained.

## Acknowledgments

The authors gratefully acknowledge support for this research from the NASA Florida Space Grant Consortium under grant NNG05 GK00H and by the U.S. Office of Naval Research under grant N00014-11-1-0068.

## References

[1] Brown, K. K., "A Concept of Operations and Technology Implications for Operationally Responsive Space," *Air and Space Power Journal* [online journal], June 2006.

[2] Stephen, A. W., and Bonnie, J. D., "Orbital Space Plane, Past, Present, and Future," *AIAA International Air and Space Symposium and Exposition: The Next 100 Years*, Dayton, OH, AIAA Paper 2003-2718, July 2003.

[3] London, H. S., "Change of Satellite Orbit Plane by Aerodynamic Maneuvering," *IAS 29th Annual Meeting*, International Astronautical Soc., New York, Jan. 1961.

[4] Walberg, G. D., "A Survey of Aeroassisted Orbit Transfer," *Journal of Spacecraft and Rockets*, Vol. 22, No. 1, 1985, pp. 3–18. doi:10.2514/3.25704

[5] Mease, K. D., "Aeroassisted Orbital Transfer: Current Status," *Journal of the Astronautical Sciences*, Vol. 36, Nos. 1–2, 1988, pp. 7–33.

[6] Hull, D. G., Giltner, J. M., Speyer, J. L., and Mapar, J., "Minimum Energy-Loss Guidance for Aeroassisted Orbital Plane Change," *Journal of Guidance, Control, and Dynamics*, Vol. 8, No. 4, 1985, pp. 487–493. doi:10.2514/3.20009

[7] Seywald, H., "Variational Solutions for the Heat-Rate-Limited Aeroassisted Orbital Transfer Problem," *Journal of Guidance, Control, and Dynamics*, Vol. 19, No. 3, May–June 1996, pp. 686–692. doi:10.2514/3.21675

[8] Vinh, N., and Shih, Y., "Optimum Multiple-Skip Trajectories," *Acta Astronautica*, Vol. 41, No. 2, July 1997, pp. 103–112. doi:10.1016/S0094-5765(97)00203-8

[9] Ross, I., and Nicholson, J., "Optimality of the Heating-Rate-Constrained Aerocruise Maneuver," *Journal of Spacecraft and Rockets*, Vol. 35, No. 3, May–June 1998, pp. 361–364. doi:10.2514/2.3335

[10] Zimmerman, F., and Calise, A. J., "Numerical Optimization Study of Aeroassisted Orbital Transfer," *Journal of Guidance, Control, and Dynamics*, Vol. 21, No. 1, Jan.–Feb. 1998, pp. 127–133. doi:10.2514/2.4208

[11] Baumann, H., and Oberle, H., "Numerical Computation of Optimal Trajectories for Coplanar, Aeroassisted Orbital Transfer," *Journal of Optimization Theory and Applications*, Vol. 107, No. 3, Dec. 2000, pp. 457–479. doi:10.1023/A:1026454013374

[12] Baumann, H., "Thrust Limited Coplanar Aeroassisted Orbital Transfer," *Journal of Guidance, Control, and Dynamics*, Vol. 24, No. 4, July–Aug. 2001, pp. 732–738. doi:10.2514/2.4773

[13] Rao, A. V., Tang, S., and Hallman, W. P., "Numerical Optimization Study of Multiple-Pass Aeroassisted Orbital Transfer," *Optimal Control Applications and Methods*, Vol. 23, No. 4, July–Aug. 2002, pp. 215–238. doi:10.1002/oca.711

[14] Trask, A., and Coverstone, V., "Optimal Low-Thrust Trajectories Combined with an Aeroassist Maneuver," *Journal of Spacecraft and Rockets*, Vol. 41, No. 4, July–Aug. 2004, pp. 629–634. doi:10.2514/1.2582

[15] Berend, N., Bertrand, S., and Jolly, C., "Optimization Method for Mission Analysis of Aeroassisted Orbital Transfer Vehicles," *Aerospace Science and Technology*, Vol. 11, No. 5, June 2007, pp. 432–441. doi:10.1016/j.ast.2007.01.007

[16] Gogu, C., Matsumura, T., Haftka, R. T., and Rao, A. V., "Aeroassisted Orbital Transfer Trajectory Optimization Considering Thermal Protection System Mass," *Journal of Guidance, Control, and Dynamics*, Vol. 32, No. 3, May–June 2009, pp. 927–938. doi:10.2514/1.37684

[17] Berend, N., and Bertrand, S., "MDO Approach for Early Design of Aerobraking Orbital Transfer Vehicles," *Acta Astronautica*, Vol. 65, Nos. 11–12, Dec. 2009, pp. 1668–1678. doi:10.1016/j.actaastro.2009.04.016

[18] Jorris, T., "Common Aero Vehicle Autonomous Reentry Trajectory Optimization Satisfying Way-Point and No-Fly Zone Constraints," Ph.D. Thesis, Air Force Institute of Technology, Wright-Patterson AFB, OH, 2004.

[19] Jorris, T. R., and Cobb, R. G., "Multiple Method 2-D Trajectory Optimization Satisfying Way-Points and No-Fly Zone Constraints," *Journal of Guidance, Control, and Dynamics*, Vol. 31, No. 3, May–June 2008, pp. 543–553. doi:10.2514/1.32354

[20] Jorris, T. R., and Cobb, R. G., "Three-Dimensional Trajectory Optimization Satisfying Waypoint and No-Fly Zone Constraints," *Journal of Guidance, Control, and Dynamics*, Vol. 32, No. 2, March–April 2009, pp. 551–572. doi:10.2514/1.37030

[21] Rao, A. V., Benson, D. A., Darby, C. L., Francolin, C., Patterson, M. A., Sanders, I., and Huntington, G. T., "Algorithm 902: GPOPS, A Matlab Software for Solving Multiple-Phase Optimal Control Problems Using the Gauss Pseudospectral Method," *ACM Transactions on Mathematical Software*, Vol. 37, No. 2, April–June 2010, Article 22, p. 39. doi:10.1145/1731022.1731032

[22] Vinh, N.-X., Busemann, A., and Culp, R. D., *Hypersonic and Planetary Entry Flight Mechanics*, Univ. of Michigan Press, Ann Arbor, MI, 1980, pp. 4–28.

[23] Betts, J. T., *Practical Methods for Optimal Control and Estimation Using Nonlinear Programming*, 2nd ed., SIAM Press, Philadelphia, 2009, pp. 372–375.

[24] Clarke, K., "Performance Optimization of a Common Aero Vehicle Using a Legendre Pseudospectral Method," M.S. Thesis, Department of Aeronautics and Astronautics, Massachusetts Inst. of Technology, Cambridge, MA, 2003.

[25] Detra, R. W., Kemp, N. H., and Riddell, F. R., "Addendum to Heat Transfer of Satellite Vehicles Re-Entering the Atmosphere," *Jet Propulsion*, Vol. 27, 1957, pp. 1256–1257.

[26] Darby, C. L., Hager, W. W., and Rao, A. V., "Direct Trajectory Optimization Using a Variable Low-Order Adaptive Pseudospectral Method," *Journal of Spacecraft and Rockets* (accepted for publication).

[27] Darby, C. L., Hager, W. W., and Rao, A. V., "An $hp$-Adaptive Pseudospectral Method for Solving Optimal Control Problems," *Optimal Control Applications and Methods* [online], Aug. 2010. doi:10.1002/oca.957

[28] Gill, P. E., Murray, W., and Saunders, M. A., "SNOPT: An SQP Algorithm for Large-Scale Constrained Optimization," *SIAM Review*, Vol. 47, No. 1, 2005, pp. 99–131. doi:10.1137/S0036144504446096

[29] Gill, P. E., Murray, W., and Saunders, M. A., "User's Guide for SNOPT Version 7: Software for Large Scale Nonlinear Programming," Stanford Univ. Optimization Lab., Palo Alto, CA, Feb. 2006.

[30] Rump, S. M., "INTLAB: INTerval LABoratory," *Developments in Reliable Computing*, edited by T. Csendes, Kluwer Academic, Dordrecht, Germany, 1999, pp. 77–104.

[31] Garg, D., Patterson, M. A., Darby, C. L., Francolin, C., Huntington, G. T., Hager, W. W., and Rao, A. V., "Direct Trajectory Optimization and Costate Estimation of Finite-Horizon and Infinite-Horizon Optimal Control Problems Using a Radau Pseudospectral Method," *Computational Optimization and Applications* [online], Oct. 2009. doi:10.1007/s10589-009-9291-0

[32] Garg, D., Patterson, M. A., Hager, W. W., Rao, A. V., Benson, D. A., and Huntington, G. T., "A Unified Framework for the Numerical Solution of Optimal Control Problems Using Pseudospectral Methods," *Automatica*, Vol. 46, No. 11, Nov. 2010, pp. 1843–1851. doi:10.1016/j.automatica.2010.06.048

[33] Tewari, A., *Atmospheric and Space Flight Dynamics*, Birkhäuser, Boston, 2007, pp. 130–138.

D. Spencer
*Associate Editor*